Magnetic Properties of the Antiferromagnet $DyPO_4$ in Applied Fields

C. S. Koonce, B. W. Mangum, and D. D. Thornton
National Bureau of Standards, Washington, D. C. 20234
(Received 13 May 1971)

The magnetization and susceptibility of the Ising antiferromagnet $DyPO_4$ have been measured as a function of temperature and applied field for samples having demagnetization factors $D \approx 0.02$ and $D \approx 1.0$. Also, the temperature at which peaks in the heat capacity at constant applied field occurred were measured for a number of applied fields. These results have been compared with predictions of the molecular-field approximation and the Bethe-Peierls approximation including long-range dipolar interactions. The temperature below which the antiferromagnetic-paramagnetic transition is first order has been obtained within the molecular-field approximation. In addition, expressions are obtained for the magnitude of the discontinuity in the heat capacity at the transition between the intermediate (or mixed) state and the antiferromagnetic or paramagnetic states for samples having nonzero demagnetization factors. These expressions do not depend on the molecular-field or Bethe-Peierls approximations.

I. INTRODUCTION

Dysprosium phosphate is a good material to use as a basis for study of three-dimensional Ising antiferromagnets. It is highly anisotropic, having g factors determined from EPR measurements[1] of $g_{\parallel} = 19.5$ and $g_{\perp} = 0.2$.

The zero-field susceptibility, heat capacity, and sublattice magnetization of $DyPO_4$ have been measured and compared[2-4] with both low- and high-temperature series expansions based on a near-neighbor-coupling-only Ising model.[5-7] Excellent agreement was obtained for $8 \times 10^{-4} < (T_N - T)/T_N < 10^{-1}$, where T_N is the antiferromagnetic (AF) to paramagnetic (PM) transition temperature in zero applied field, indicating that in zero applied field a near-neighbor-coupling-only Ising model is a good approximation. From those measurements of susceptibility and heat capacity over a wide range of temperature, the antiferromagnetic nearest-neighbor coupling J_a/k has been determined to be 1.25 ± 0.02 K while the value obtained from spectroscopic measurements is 1.32 ± 0.07 K.[3]

In contrast to the zero-field results, the properties of $DyPO_4$ in an applied magnetic field H_0 are not well approximated by only nearest-neighbor coupling.[8] We have found that its magnetic behavior is qualitatively that expected of a two-sublattice antiferromagnet in which dipolar interactions are important. At temperatures below the Néel temperature, $T_N = 3.390$ K, $DyPO_4$ is in its AF state for fields below its critical field which depends on temperature. Also, the transition from the AF state to the PM state is first order below a critical temperature $T_c = 0.75$ K, and higher order for higher temperatures.

$DyPO_4$ has the zircon crystal structure[9] which consists of linked DyO_4 and PO_4 tetrahedra with common oxygen atoms. The symmetry is tetragonal and the space group is D_{4h}^{19} ($I4_1/amd$), and the unit-cell dimensions are $a_0 = 6.917$ Å and $c_0 = 6.053$ Å. The four magnetically equivalent Dy^{3+} ions per unit cell have a site symmetry D_{2d}. A given Dy^{3+} ion has four nearest neighbors which lie at the apices of a flattened tetrahedron. The magnetic crystal structure of $DyPO_4$ can be constructed from two interpenetrating body-centered-tetragonal lattices which form the two sublattices of the antiferromagnetic state shown in Fig. 1, where the four nearest neighbors lie on the opposite sublattice from that of a given ion.

We have measured the magnetization of $DyPO_4$ samples having demagnetization factors $D \approx 0.02$ and $D \approx 1.0$, the former to obtain the properties of a long needle and the latter to compare with maxima in the heat capacity at constant applied field for various fields. The heat capacity was measured with a sample having a demagnetization factor $D \approx 1.0$, in order for the sample to have a volume large enough for us to measure its heat-capacity maxima.

In order to understand the qualitative dependence

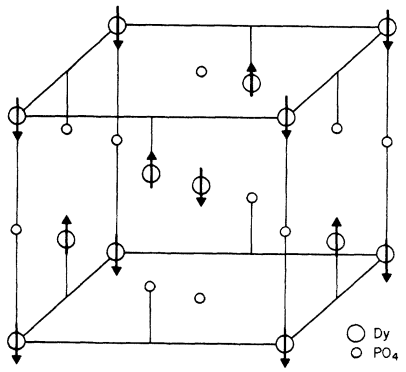

FIG. 1. Antiferromagnetic state of $DyPO_4$.

of the magnetization and heat-capacity maxima on field and temperature, we have compared the experimental results with a molecular-field theory including dipolar interactions, and a Bethe-Peierls theory including long-range dipolar interactions.

Equations for the magnetization and heat capacity of an antiferromagnet having near-neighbor coupling and dipolar coupling are given in Sec. II using molecular-field and Bethe-Peierls approximations. These developments are made together so that the reader may compare the approximations made in the two approaches. Also, calculations of the magnetization and heat capacity are made using both approximations so that each may be compared with the measurements on $DyPO_4$. Also in Sec. II the molecular-field position of the critical temperature T_c as a function of the ratio of the intrasublattice to the antiferromagnetic intersublattice interactions is given for all ferromagnetic values of the intrasublattice interaction.

Section III contains a description of the measurements made on $DyPO_4$ and of sample preparations. Section IV contains a discussion of the measurements made with $D \approx 0.02$ and comparison is made with the models developed in Sec. II.

In Sec. V a description of the intermediate or mixed state is given, and special attention is given to calculating the directly measured quantities such as the heat capacity at constant applied field in the intermediate state and for the discontinuity in heat capacity on crossing the boundary of the intermediate state. An equation for the location of the Schottky maximum in the H-T plane is also given.

These expressions are used in Sec. VI to compare the magnetization and thermal measurements with each other and with the molecular-field and Bethe-Peierls approximations for samples of $DyPO_4$ having approximate demagnetization factors near unity.

II. MOLECULAR-FIELD AND BETHE-PEIERLS APPROXIMATIONS

We will now consider a two-sublattice Ising antiferromagnet having both dipolar and exchange interactions. We will then make molecular-field and Bethe-Peierls approximations separately. The Hamiltonian for such a system is

$$\mathcal{H} = J_a \sum_{\langle R,\beta\rangle} S(R)S(R+\beta) + \tfrac{1}{2}\sum_{R,R'} J^d_{RR'}\, S(R)S(R') + \tfrac{1}{2}\sum_{R,R'} J^e_{RR'} S(R)S(R') - \mu H_0 \sum_R S(R)\,, \qquad (1)$$

where $\mu = \frac{1}{2} g \mu_B$ and J_a is the total antiferromagnetic nearest-neighbor interaction, dipolar plus exchange, $J^d_{RR'}$ is the dipolar interaction, $J^e_{RR'}$ is the exchange interaction between ions at R and R', with R and R' never nearest neighbors, and $H_0 = B_0$ is the applied field. The notation $\langle R, \beta\rangle$ indicates a sum over pairs R and $R+\beta$, and $S(R)$ takes on the values ± 1.

If we consider a large sphere centered at R and use the fact that $J^e_{RR'} \to 0$ faster than $|R-R'|^{-3}$, we have

$$\mathcal{H} = J_a \sum_{\langle R,\beta\rangle} S(R)S(R+\beta) + \tfrac{1}{2}\sum_{(R,R')} (J^d_{RR'} + J^e_{RR'})S(R)S(R') + \tfrac{1}{2}\sum_{)R,R'(} J^d_{RR'}\, S(R)S(R') - \mu H_0 \sum_R S(R)\,, \qquad (2)$$

where the sum (R, R') contains all R' except nearest neighbors in a large sphere centered about R and $)R, R'($ contains all R' outside the sphere. This sum may be replaced by an integral, leading to

$$\mathcal{H} = J_a \sum_{\langle R,\beta\rangle} S(R)S(R+\beta) + \tfrac{1}{2}\sum_{(R,R')} (J^d_{RR'} + J^e_{RR'})S(R)S(R') - \tfrac{1}{2}\mu(D_0 - D)M \sum_R S(R) - \mu H_0 \sum_R S(R)\,, \qquad (3)$$

where D_0 is the demagnetization factor for a sphere, $4\pi/3$, and M is the magnetization.

We can proceed by two alternate methods. We may treat all terms in the molecular-field approximation or we may neglect the second term and treat the first and last two terms using a modified Bethe-Peierls method. The molecular-field method has the advantage of including all interactions although they are all treated in an approximate manner. These approximations are expected to give the largest errors when treating the relatively strong interactions of nearest neighbors.

To use the molecular-field approximation, we define

$$\mu H_i^{\,j} = \sum_{R_i'} J^j_{RR_i'} \qquad (4)$$

and

$$m' = \langle S(R)\rangle = \frac{2M'}{M_0} = \frac{2}{N}\sum_{R_1} S(R_1)\,, \qquad (5)$$

where the subscript i is 1 when the sum over R' is on the same sublattice as R, and 2 when the sublattice is the opposite sublattice, again excluding nearest neighbors. The superscript j refers to either exchange or dipolar interactions. For example, H_1^d is the dipolar field arising from all ions on the same sublattice inside a large sphere in the PM state at $T=0$, and H_2^d is the dipolar field arising from all ions on the opposite sublattice inside a large sphere excluding nearest neighbors in the PM state at $T=0$. M' is the magnetization of one sublattice, and $M = M' + M''$, $m = \frac{1}{2}(m' + m'') = M/M_0$; and M_0 is the saturation magnetization.

The energy per spin in the molecular-field approximation is then

$$U_{MF} = \tfrac{1}{2}\{[zJ_a + \mu H_2^d + \mu H_2^e + \tfrac{1}{2}(D_0 - D)M_0]m'm'' + \tfrac{1}{2}[\mu H_1^d + \mu H_1^e + \tfrac{1}{2}(D_0 - D)M_0](m'^2 + m''^2) - \mu H_0(m' + m'')\}\ , \quad (6)$$

where z is the number of nearest neighbors of a given ion and m' and m'' are the reduced sublattice magnetizations $2M'/M_0$, $2M''/M_0$, with $0 \le m' \le 1$ and $-1 \le m'' \le 1$.

The effective fields on these individual sublattices are then

$$H' = H_0 - H_a m'' + H_p m'\ , \quad (7a)$$

$$H'' = H_0 - H_a m' + H_p m''\ , \quad (7b)$$

with

$$H_a = (zJ_a/\mu) - H_2^d - H_2^e - \tfrac{1}{2}(D_0 - D)M_0\ , \quad (8a)$$

$$H_p = H_1^d + H_1^e + \tfrac{1}{2}(D_0 - D)M_0\ . \quad (8b)$$

We then find that $kT_N = \mu H_a + \mu H_p$, and for a long needle $H_a = H_c(0)$, the critical field at zero temperature. We define

$$\lambda = (1 - \mu H_a/kT_N) = H_p/(H_a + H_p)\ , \quad (9)$$

which for $DyPO_4$ gives $\lambda = 0.32 \pm 0.03$. This becomes $\lambda = 0.34$ when we make the approximations $H_1^d \approx -H_1^e$, $H_2^d \approx -H_2^e$. The equations for the sublattice magnetization in terms of λ are

$$m' = \tanh\left[\frac{(1-\lambda)h - (1-\lambda)m'' + \lambda m'}{t}\right], \quad (10a)$$

$$m'' = \tanh\left[\frac{(1-\lambda)h - (1-\lambda)m' + \lambda m''}{t}\right], \quad (10b)$$

where $h = H_0/H_c(0)$ and $t = T/T_N$. The solution in the PM state is given by $m' = m'' = m = M/M_0$.

The sum of all exchange interactions between a given ion and all ions on the other sublattice may be calculated from a knowledge of the critical field at zero temperature. The energies per spin of the PM and AF states for a long needle at $T = 0$ are

$$E_p = \tfrac{1}{2}[zJ_a - D_0M_0 - \mu(H_1^d + H_1^e + H_2^d + H_2^e) - 2\mu H_0]\ , \quad (11)$$

$$E_a = \tfrac{1}{2}[-zJ_a - \mu(H_1^d + H_1^e) + \mu(H_2^d + H_2^e)]\ . \quad (12)$$

Note that the sign of all fields is such that a positive value of the field corresponds to a ferromagnetic interaction. By equating these energies we obtain the critical field at zero temperature

$$H_c(0) = zJ_a/\mu - \tfrac{1}{2}D_0M_0 - H_2^d - H_2^e\ . \quad (13)$$

The value of the critical field at zero temperature, $H_c(0)$, for the transition from the AF state into the PM state (often called the metamagnetic transition) is 5.45 kG, as obtained from our magnetization measurements. The value obtained from a near-neighbor-coupling-only calculation is $H_c(0) = zJ_a/\mu = 7.67$ kG, or 8.07 kG, depending on the value of J_a taken, where z is the number of nearest neighbors (4) and $\mu = \frac{1}{2}g\mu_B = 0.6515$ K/kG. The inclusion of long-range dipolar interactions (the Lorentz field) only, gives $H_c(0) = (zJ_a/\mu - \frac{1}{2}D_0M_0) = 5.06$ kG or 5.46 kG again depending on the value of J_a taken. In addition, the inclusion of the dipolar interactions leads to a first-order transition at low temperatures, as is observed experimentally.

Since $H_c(0) = 5.45 \pm 0.01$ kG, and $J_a/k = 1.25 \pm 0.02$ K and H_2^d was obtained from a dipole sum (see Table I), we may use Eq. (13) to determine $H_2^e = -1.63 \pm 0.04$ kG, which differs from the result of Ref. 3 of $H_2^e = -0.97 \pm 0.52$ kG which was based on optical measurements. The value of H_1^e given in Table I is taken from Ref. 3 and is based on optical measurements. We see from Table I that H_1^d and H_1^e have opposite signs, as do H_2^d and H_2^e. This partial cancellation of the dipolar and exchange interactions for other than nearest neighbors explains why a model having only near-neighbor interactions (dipolar plus exchange) of $J_a/k = 1.25$ K describes $DyPO_4$ so well in zero applied field. It also indicates that a model having the same near-neighbor interactions and long-range dipolar interactions outside a sphere should be a good approximation for $DyPO_4$. In addition, as we show in Appendix A, the dipolar and exchange fields from the second- through fifth-near-neighbor interactions have opposite signs individually as well.

In all model calculations presented in this paper, both molecular-field and Bethe-Peierls, we have assumed complete cancellation of H_1^d and H_1^e, and H_2^d with H_2^e. Within the molecular-field model, if we express all properties in terms of the reduced units $h = H_0/H_c(0)$ and $t = T/T_N$ the only material-dependent parameter is λ. The molecular-field calculations are easily corrected to include the lattice sums by changing the value of λ. The approximation we use, therefore, is one that is strictly suited to a cubic Ising system with dipolar interactions and nearest-neighbor exchange interactions only. The only difference between this approximation and our approximation for $DyPO_4$ is that for $DyPO_4$, J_a is the sum of dipolar and exchange interactions between nearest neighbors, while for the cubic lattice mentioned above, J_a is the exchange interaction only, since in that case the total dipolar interaction is zero.

Let us now consider an Ising antiferromagnet in the shape of a long needle (demagnetization factor $D = 0$) in an external field applied along the direction of alignment of the Ising system, which is also the principal axis of the needle. For small $t = T/T_N$,

TABLE I. Dipolar fields at an ion on the A sublattice. $H_1^q = 0.112$ kG; $H_2^q = 1.23$ kG; $\alpha = 3.4585$ Å; $a = 6.917$ Å; $H_1^e = -0.12$ kG; $H_2^e = -1.63$ kG; $\gamma = 1.5132$ Å; $c = 6.053$ Å. A plus sign indicates a ferromagnetic interaction.

Neighbor	Position of one neighbor	Sublattice	Distance from central ion (Å)	Number of neighbors	Total dipolar field (kG)
1	$(0, \alpha, \gamma)$	B	3.775	4	−3.491
2	$(\alpha, 0, 3\gamma)$	B	5.707	4	+1.752
3	$(\alpha, \alpha, 2\gamma)$	A	5.752	8	−0.645
4	$(0, 0, c)$	A	6.053	2	+1.635
5	$(0, a, 0)$	A	6.917	4	−1.096
6	(a, α, γ)	B	7.880	8	−1.318
7	$(0, \alpha, c+\gamma)$	B	8.319	4	+0.933
8	$(\alpha, a, 3\gamma)$	B	8.967	8	−0.232
9	$(0, a, c)$	A	9.192	8	+0.281
10	$(a, a, 0)$	A	9.782	4	−0.387

the transition from the AF state into the PM state in a field will be first order if there is a net ferromagnetic interaction between ions on the same sublattice. In $DyPO_4$, this interaction is principally the dipolar interaction with distant neighbors. A molecular-field calculation predicts that the first-order transition will occur up to a temperature $t_c(\lambda)$ shown in Fig. 2. For $\lambda \geq \frac{3}{8}$ the first-order transition occurs between the AF and PM states and the first-order transition becomes second order at[11,10] $t_c(\lambda) = \frac{4}{3} - 1/3\lambda$. For $\lambda < \frac{3}{8}$ the first-order transition line extends into the AF state; that is, at some temperatures there is a first-order transition between two AF states followed by a second-order transition into the PM state as the applied field is increased.[10,12] In this case, the first-order transition ends in a critical point and the temperature of this point is $t_c(\lambda) > \frac{4}{3} - 1/3\lambda$. A phase diagram in the H-T plane is shown in Fig. 3 using the molecular-field approximation and $\lambda = 0.34$. For this value of λ, corresponding to the interactions in $DyPO_4$, the first-order transition occurs within the AF state over only a very narrow temperature range.

For small λ the critical point occurs at low temperatures and the hyperbolic tangent may be approximated by unity in Eqs. (10) for the sublattice magnetization which is in the direction of the applied magnetic field. Thus, in the small λ limit, one sublattice magnetization is saturated and the other sublattice magnetization is zero at the critical point and the temperature of that critical point is

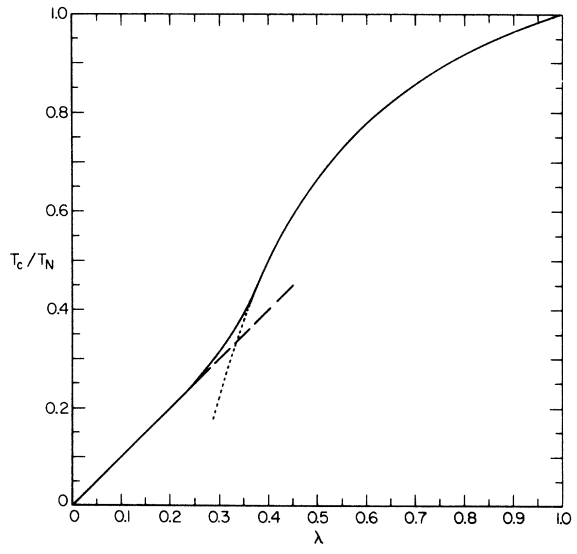

FIG. 2. Reduced critical temperature $t_c = T_c/T_N$ as a function of λ. The dotted line is given by $t_c(\lambda) = \frac{4}{3} - 1/3\lambda$ which is exact above $\lambda = \frac{3}{8}$. The dashed line is $t_c(\lambda) = \lambda$. The solid curve is obtained numerically.

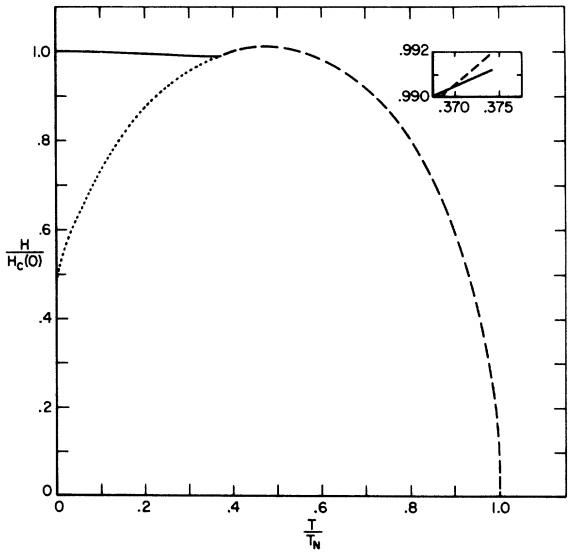

FIG. 3. Phase diagram of $DyPO_4$ using the molecular-field approximation with $D = 0$ and $\lambda = 0.34$. The solid curve is the first-order transition, and the dashed curve is the second-order transition. The dotted curve does not represent a transition. The region near the critical point is shown in the inset.

$t_c(\lambda)=\lambda$ (as $\lambda \to 0$). The critical-point temperature approaches λ from above, so that $t_c(\lambda) \geq \lambda$ for $\lambda \geq 0$. For $\lambda < \frac{1}{4}$ the approximation $t_c(\lambda) \approx \lambda$ is very good. The whole curve of $t_c(\lambda)$ is fairly well approximated by the greater of $\frac{4}{3} - 1/3\lambda$ or λ (see Fig. 2).

The low-temperature (small λ) approximation to the critical point in the molecular-field approximation is interesting because of its simplicity. In this approximation we have $m' \approx 1$, $H_0 \approx H_c(0)$, and $m'' \approx \tanh(\lambda m''/t)$, which has two solutions corresponding to the two AF states for $t < \lambda$, and no solution for $t > \lambda$. We note that the equation for the *sublattice* magnetization m'' is equivalent to the equation for the total magnetization m of a ferromagnet, and the different branches of the solution for m'' (positive and negative) are achieved for applied fields infinitesimally greater than or less than the critical field, respectively.

While the above results are those obtained in a molecular-field approximation, we shall suppose that the qualitative result of a first-order transition occurring for temperatures less than a critical temperature t_c is valid for systems with AF near-neighbor coupling and ferromagnetic long-range dipolar coupling.[10–22] This behavior is observed in $DyPO_4$.

The molecular-field prediction of a second-order transition at applied fields higher than the first-order transition field has not been observed, and, in fact, comparison with two-dimensional Ising model solutions[23] leads one to take the inflection point of the M-vs-H_0 curves at constant T as the phase transition. This method was used to obtain the experimental phase diagram shown as squares in Fig. 4. The molecular-field calculation predicts that the maximum of $(\partial M/\partial H)_T$ is inside the AF region. This maximum is closer to the actual transition than is the predicted second-order transition.

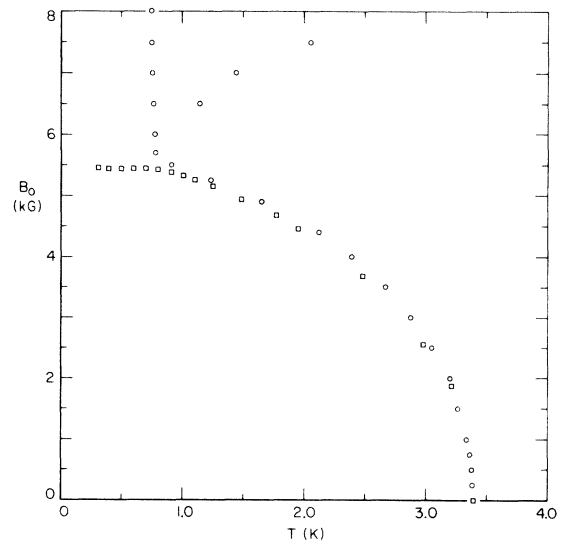

FIG. 4. Phase diagram of $DyPO_4$. The squares are obtained from peaks in the susceptibility for a long needle, $D \approx 0.02$, and the circles are from maxima in the heat capacity at constant applied field of a sample having $D \approx 1$. The locus of the Schottky maximum is also shown.

Since we have an Ising system we would expect that the molecular field would provide a good approximation to the real system at low temperatures. There are, however, only four magnetic nearest neighbors which are strongly coupled to the central ion, so we would expect the Bethe-Peierls approximation (which for our Ising system is the same as a constant coupling approximation)[24] to be significantly better than the molecular-field approximation.

In order to use the Bethe-Peierls approximation we will approximate the sum in Eq. (3):

$$\sum_{(R,R_i')} (J^a_{RR_i'} + J^e_{RR_i'}) \approx 0 \tag{14}$$

for $i = 1$ or 2, so that

$$\mathcal{H}_{BP} = J_a \sum_{(R,\beta)} S(R)S(R+\beta) - \mu[H_0 + (D_0 - D)M_0] \sum_R S(R) , \tag{15}$$

which leads to the Hamiltonian of a cluster of ions about an ion on the α sublattice

$$\mathcal{H}_\alpha = J_a \sum_\beta S(R)S(R+\beta) + \mu H' \sum_\beta S(R+\beta) - \mu[H_0 + (D_0 - D)M]S(R) + \mu H'' \sum_\alpha S(R+\alpha) , \tag{16}$$

where H' and H'' are fictitious fields to be determined self-consistently from consideration of the cluster centered at $R+\beta$, on the other sublattice.

If we define

$$y = \exp(-2J_a/kT) ,$$

$$s = \exp\{-2\mu[H_0 + (D_0 - D)M]/kT\} ,$$

$$\epsilon = \exp(-2\mu H'/kT) ,$$

$$B = (\epsilon + y)/(1 + \epsilon y) ,$$

and set up equations in the paramagnetic region where the expectation value of a spin is the same on both sublattices, we obtain[25]

$$\epsilon = 1/sB^{z-1} \tag{17a}$$

or

$$B(y + sB^{z-1}) = 1 + syB^{z-1} . \tag{17b}$$

If dipolar interactions had been neglected, we

could solve Eq. (17a) or (17b) for ϵ or B and obtain the magnetization from the relation

$$m = M/M_0 = (1 - sB^s)/(1 + sB^s) \ . \tag{18}$$

When dipolar interactions are included, we have the result that Eqs. (17) depend on m so that Eqs. (17) and (18) must be solved simultaneously for B and M. Eliminating B and defining $\delta = [(1-m)/(1+m)]^{1/s}$ and $\gamma = s^{1/s}$, we have

$$\delta y \gamma^{-1} + \delta^s - y\gamma\delta^{s-1} - 1 = 0 \ , \tag{19}$$

which can be solved numerically for δ and, hence, m as a function of applied field and temperature.

The expectation value of the energy in the constant-coupling approximation is[26]

$$\frac{\langle E \rangle}{N} = \tfrac{1}{2} z J_a - z J_a \left[\frac{1 - [1 - (1-m^2)(1-y^2)]^{1/2}}{1-y^2} \right] - \mu H_0 m - \tfrac{1}{2} \mu (D_0 - D) M_0 m^2 \ . \tag{20}$$

By taking the derivative of Eq. (20) at constant applied field we can obtain the heat capacity at constant applied field in the Bethe-Peierls approximation.

III. EXPERIMENTAL PROCEDURES

The crystals of $DyPO_4$ were prepared according to the method of Feigelson[27] by J. C. Wright of John Hopkins University. They were good optical-quality crystals and free of inclusions. They were typically in the shape of parallelepipeds of approximate dimensions $1 \times 1 \times 4$ mm with the optic axis lying along the long direction of the crystal. Attempts to fashion ellipsoidal samples from the parallelepipeds were unsuccessful since the crystals are very brittle and cleave readily into needles. As a result, we were forced to use nonellipsoidal-shaped samples in our experiments.

The cryostat used in making the magnetization, the differential susceptibility, and some of the heat-capacity measurements was a top-loading ^3He refrigerator. The majority of the heat-capacity measurements, however, were made in an adiabatic-demagnetization cryostat.

Magnetization isotherms were obtained for single-crystal specimens of $DyPO_4$ in fields up to 22 kG at temperatures between 0.3 and 4.2 K. The isotherms were obtained quasistatically using a continuously recording vibrating-sample magnetometer[28] which utilized a piezoelectric element as the vibrator and which was located in the cryostat. After amplification, the signal from the pickup coils was fed into a phase-sensitive detector, the output of which was fed into the Y input of an X-Y recorder. The horizontal, X, axis of the recorder was driven by a voltage directly proportional to the applied magnetic field provided by a laboratory electromagnet. The measurements were made on parallelepiped-shaped single crystals whose demagnetization factors D were approximately 1.0 or 0.02. Since the crystals were not ellipsoidal in shape the fields inside the crystals were not uniform throughout and, hence, strictly speaking, there is not a unique demagnetizing factor. If one assumes that the crystals approximate an ellipsoidal shape, however, one can calculate a demagnetization factor which should be a fairly good approximation to that of the real crystals. We find that the experimental determination of the demagnetization factor, determined from the slope of the magnetization curves in the first-order region, is in agreement with that calculated in this way.

The crystals were mounted in the magnetometer such that the tetragonal axis, the axis of spin alignment, was along the direction of vibration and also along the direction of the applied field.

During the experiments the magnetic field could be swept at any desired rate between 0 and 10^4 G/min. As a practical matter it was not convenient to sweep the field at a rate of less than 5 G/min. At the very low temperature there was considerable hysteresis for the crystal with $D \approx 0.02$ even for a sweep rate of 5 G/min. The crystal with a demagnetization factor $D \approx 1$, however, showed no hysteresis in its magnetization curve.

Measurements of the differential susceptibility $\partial M/\partial H$ were obtained by an ac bridge technique, i.e., using an Hartshorn bridge, in fields up to 22 kG between the temperatures of 0.3 and 4.2 K. The secondary coil of the mutual-inductance pair was wound as a quadrupole coil in order to minimize pickup. The entire coil assembly was rather small; its dimensions were 1.60 long and 8 mm in diameter. The primary contained 1510 turns of AWG 48 copper wire and the secondary contained 920 turns of AWG 48 copper wire. Measurements were made as a function of frequency in the range 20–1000 Hz on a $DyPO_4$ single crystal which was mounted on a platform such that it was located at the middle of the pickup coil and such that the tetragonal axis of the crystal was along the axis of the coil. This was also the direction of the applied field. At a given temperature the measurements of $\partial M/\partial H$ were made on a point-by-point basis, rather than continuously recording $\partial M/\partial H$ while varying the field. In some cases measurements of $\partial M/\partial H$, either point by point or continuously recording the values, provide a very illuminating way of displaying the data.

The phase diagram of $DyPO_4$ can be obtained not only from the magnetization at various temperatures but also from a study of the heat capacity in a variety of applied fields. We have made a determination of the temperatures of the maxima in the heat capacity in a constant applied magnetic field, which was directed along the tetragonal axis of the

single crystal, by monitoring the temperature of a thermometer in good thermal contact with the crystal while heating the crystal at a uniform rate. The thermometer was a carbon resistor which had been previously calibrated against cerous magnesium nitrate and chromic potassium alum magnetic thermometers, which, themselves, had been calibrated against the liquid-^{4}He vapor pressure scale.[29] Corrections were made for magnetoresistive effects of the carbon resistor. The thermometer was varnished directly on the crystal which, in turn, was varnished to the heater. The entire assembly was suspended by fine cotton threads in a vacuum jacket. A weak thermal link from the assembly to the outside helium bath was provided by a fine copper wire, one end of which was varnished to the heater and the other end soldered to the shield which was in contact with the bath. The bonding agent used was GE 7031 varnish.[30] The crystal of $DyPO_4$ used for the measurements had a demagnetization factor of $D \approx 1$. Although we were unable to obtain values of the heat capacity by this procedure, we could readily obtain the temperatures of the maxima. The locus of such maxima gives the phase diagram in the B_0-T plane, and the locus of Schottky maxima.

IV. DISCUSSION OF $D=0$ RESULTS

Typical measurements of magnetization as a function of applied field for temperatures ranging from 0.50 to 4.20 K are shown in Fig. 5 for a long needle of $DyPO_4$, $D \approx 0.02$. The AF-PM transition was taken to be the position of maximum slope.

In general, with $T/T_N \ll 1$ one would expect, for

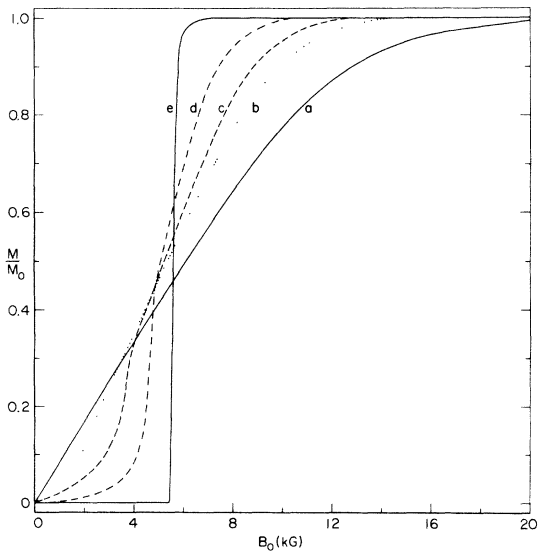

FIG. 5. Magnetization as a function of applied field at the temperatures *a*, 4.20 K; *b*, 2.97 K; *c*, 2.48 K; *d*, 1.77 K; *e*, 0.498 K.

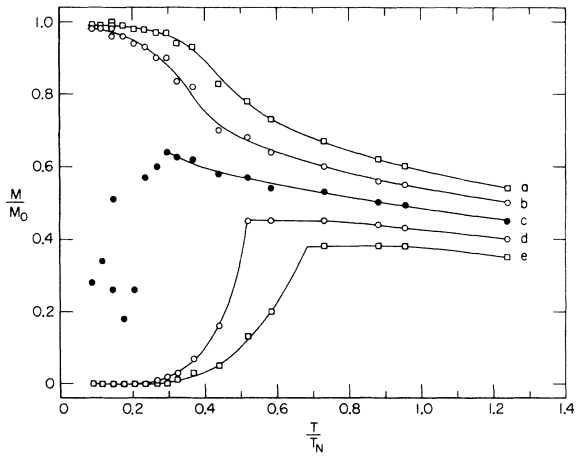

FIG. 6. Magnetization as a function of temperature for different applied fields H_0: *a*, 6.45 kG; *b*, 6.00 kG; *c*, 5.45 kG; *d*, 4.90 kG; *e*, 4.36 kG, giving $H_0/H_c(0)$ values of approximately 1.2, 1.1, 1.0, 0.9, and 0.8.

a metamagnetic system, that $(\partial M/\partial H)_T$ would be quite small but increasing as the field is increased until reaching a peak at a certain field, the critical field required to cause the system to go from the antiferromagnetic state to the paramagnetic state. At that field the peak is very sharp and high if the transition is of first order, as expected at low temperatures for crystal having dipolar interactions and whose $D=0$ or very small. For crystals with D finite and $T/T_N \ll 1$, $(\partial M/\partial H)_T$ would increase very rapidly at the critical field and then become constant until saturation of the magnetization is reached where $(\partial M/\partial H)_T$ goes to zero. At higher temperatures where the transition is greater than first order, then $(\partial M/\partial H)_T$ would be expected to have a sharp peak at the critical field, although its magnitude might not be very large and would vary with temperature.

Although the behavior described above was expected for $DyPO_4$ something entirely different was in fact observed. No sharp peaks were observed in direct measurements of the susceptibility $\partial M/\partial H$ in a field; only rounded shoulders were obtained which at low temperatures became difficult to discern. In addition, the maximum value of $\partial M/\partial H$ began descreasing, instead of continuing to increase, at approximately 1 K. At 0.75 K, the maximum value of $\partial M/\partial H$ was approximately 0.7 times that in zero applied field at 4.2 K and it decreased rapidly with decreasing temperature. At $T=0.3$ K, $\partial M/\partial H$ was essentially zero for all fields between 0 and 22 kG.

From the series of M-vs-H_0 measurements, the magnetization could be obtained as a function of T. This is shown in Fig. 6 for fields above and below the critical field evaluated at zero temperature,

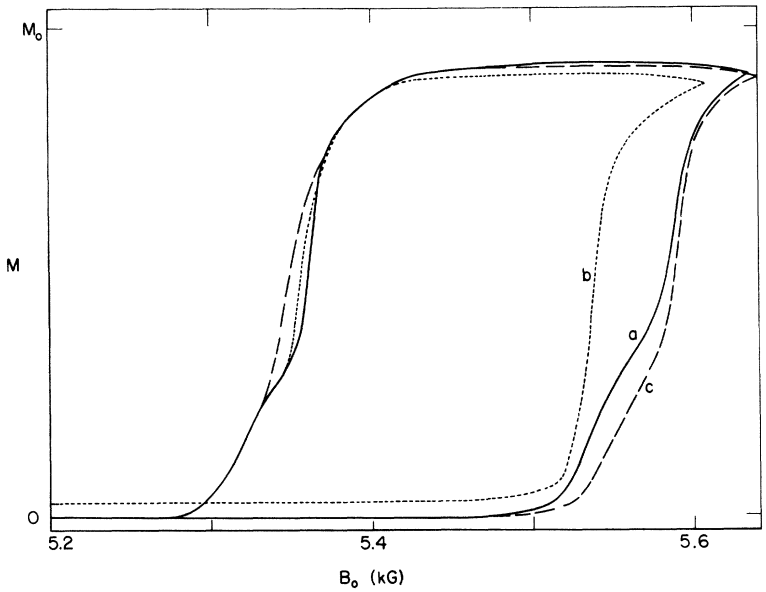

FIG. 7. Magnetization as a function of applied field at $T = 0.310$ K and demagnetization factor $D \approx 0.02$ for different sweep rates: *a*, 5 G/min; *b*, 10 G/min; *c*, 20 G/min.

$H_c(0)$. The solid curves are simply fits to the experimental points. No curve was drawn through the points below $T/T_N = 0.3$ for applied fields of $H_0 = 5.45$ kG, because the hysteresis observed for the long needle ($D = 0.02$) made determination of the magnetization near the first-order transition quite uncertain.

The hysteresis in the magnetization versus applied field curves observed for the $D = 0.02$ sample is shown in Fig. 7 for different sweep rates. The shape of the curve may indicate the presence of ferrimagnetic states[31] stable near H_c such as those discussed in Appendix A. The transition was observed to be first order up to a temperature of about 0.75 K, i.e., $T_c/T_N = 0.22$, which is smaller than the predicted value for $\lambda = 0.32$ obtained from the molecular-field approximation (Fig. 2) of $T_c/T_N = 0.34$ (or $T_c/T_N = 0.375$ for $\lambda = 0.34$). The three curves shown in Fig. 7 were obtained by first sweeping the field up from 5.0 kG and then back down at the rates indicated. The starting field of 5.0 kG was determined from faster sweep rates, in this case 50 G/min. At 50 G/min, the magnetization on the low-field side of the transition field remains to fairly low fields at the value shown at 5.0 kG for the 10-G/min sweep for increasing fields. This is probably indicative of ferrimagnetic states in the system. After locating the range of the transition field with the 50-G/min sweep, the field was increased from 5.0 to 5.6 kG and then decreased again to 5.0 kG at 10 G/min. The magnetization at 5.0 kG was then zero. We then swept the field at 20 and 5 G/min, respectively, obtaining the curves shown in Fig. 7. In each case, the magnetization was zero at 5.0 kG. Note that curve *b* (10-G/min sweep rate) does not have the shoulder that is present in curves *a* and *c* for increasing fields, i.e., at ~ 5.55 kG .

The qualitative behavior of $M(T)$ in the molecular-field calculation is shown in Fig. 8 for $\lambda = 0.34$. The notch in the curve for $H_0 = H_c$ arises from the molecular-field prediction of a second-order transition into the AF state as the temperature is lowered and then another second-order transition back into the PM state (see Fig. 3). The magnetization approaches saturation for $H = H_c(0)$ since $H_c(T) \leq H_c(0)$, where $H_c(T)$ is the temperature-dependent first-order phase-transition field. The second-order phase-transition field actually increases with increasing temperature for low temperatures in the molecular-field approximation for $\lambda > 0$, and

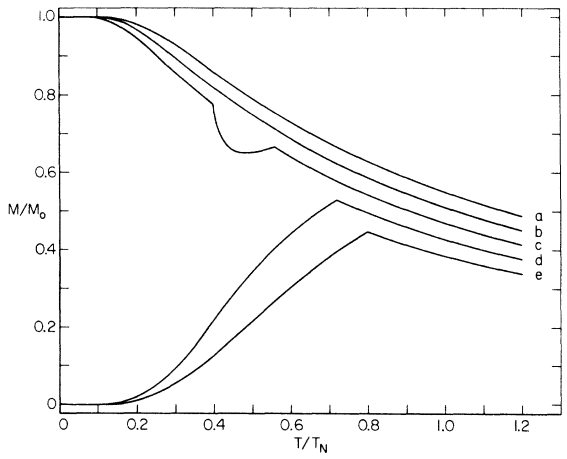

FIG. 8. Magnetization as a function of temperature in the molecular-field approximation for different applied fields $H_0/H_c(0)$: *a*, 1.2; *b*, 1.1; *c*, 1.0; *d*, 0.9; *e*, 0.8.

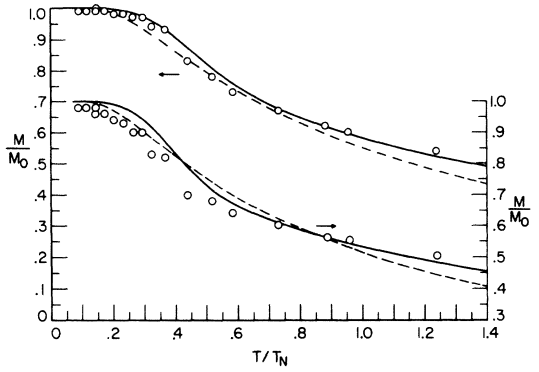

FIG. 9. Reduced magnetization as a function of reduced temperature in the Bethe-Peierls approximation (solid lines) and molecular field (dashed lines) using $J_a/k = 1.25$ K and $M_0 = 1.249$ kG compared with experimental points for $H_0/H_c(0) = 1.20$, top drawing left scale, and $H_0/H_c(0) = 1.10$, bottom drawing right scale.

decreases for higher temperatures, leading to the notch discussed above. We note that the quantitative agreement of $DyPO_4$ with the molecular-field theory is not good.

A somewhat better agreement is obtained using the Bethe-Peierls approximation. A comparison between this approximation (solid line) and experimental points for $H/H_c(0) = 1.1$ and 1.2 is shown in Fig. 9.

We note that the $D \approx 0$ magnetization measurements as well as the predictions of the molecular-field and Bethe-Peierls approximations for $D = 0$ give smooth magnetization curves as a function of temperature except for the transition between the AF and PM states. This indicates that the heat capacity should contain only one Schottky peak for fields larger than the critical field and $D = 0$.

V. SHAPE EFFECTS

In order to obtain a sufficient volume of crystal to measure the heat capacity, samples with reasonably large demagnetization factors D are usually used. While it should be possible to reduce the measurements to what they would have been for a long needle,[32,33] an analysis of heat capacity and the associated magnetization on $D \neq 0$ samples is of interest because they are measured directly and can be interpreted without recourse to transformations involving the other quantities such as the isothermal susceptibility which must be experimentally determined.

In Sec. II, we have set up equations in the molecular-field approximation which include shape effects from ellipsoidal samples entering through the demagnetization factor D.

The region of the phase diagram near the first-order phase transition (for $D = 0$) must be considered in detail. At $T = 0$, when the applied field is small, the crystal is in the AF state with $M = 0$ and H_i, the internal field, is equal to the applied field. When the applied field reaches $H_c(0)$ it becomes energetically favorable for a long needle to go into the PM state, but not energetically favorable for the ellipsoid, since the internal field $H_i = H_0 - DM_0$ in the PM phase. We would then expect that for $H_c(0) < H < H_c(0) + DM_0$ the crystal would consist of a mixture of AF and PM domains, the fraction of the crystal in the PM state increasing as the field is increased.[34] As the temperature is increased the width of this region intermediate between the AF and PM states decreases and is given by $H_c(T) + DM_a(H_c, T) < H < H_c(T) + DM_p(H_c, T)$. We shall call this region of the H-T plane consisting of a mixture of AF and PM states the intermediate state.

The properties of the intermediate state may be obtained in a number of ways. One way is to define a pseudo-free-energy F_A[33]:

$$dF_A = -SdT - MdH_i \,, \tag{21}$$

$$F_A = F + \tfrac{1}{2} DM^2 \,, \tag{22}$$

where $H_i = H_0 - DM$. The function $F_A(H_i, T)$ is the same function of local field and temperature for all shapes. If we consider a first-order transition, the internal field $H_i = H_c(T)$ is independent of applied field H_0 within the intermediate region. The free energy in the intermediate region is given by

$$F(H_0, T) = F_a(H_c, T) - \tfrac{1}{2} DM^2 = F_a(H_c, T) - \frac{(H_0 - H_c)^2}{2D} \,, \tag{23}$$

$$dF = -SdT - MdH_0 \,, \tag{24}$$

where we have used the fact that in the intermediate state the magnetization $M = [H_0 - H_c(T)]/D$. The free energy given in Eq. (23) is shown in Fig. 10 for $DM_0/H_c = \frac{1}{2}$ and $T = 0$, and we can see that for $H_c < H < H_c + DM_0$ the intermediate state is stable at $T = 0$. By taking derivatives of this free energy with respect to the applied field and temperature one can obtain the results that the entropy and magnetization are continuous at the boundary of the intermediate state; that is, the first-order transition with $D = 0$ becomes two second-order transitions with $D \neq 0$. The entropy in the intermediate state is given by

$$S(H_0, T) = S_a(H_c, T) + D[M - M_a(H_c, T)]\left(\frac{\partial M}{\partial T}\right)_{H_0} \,, \tag{25}$$

where S_a is the entropy of the antiferromagnetic state evaluated on the boundary of the intermediate state, and M_a the corresponding magnetization. Equation (25) holds also if a is replaced by p, with M_p being the magnetization of the paramagnetic

(or second AF) state. In the intermediate state we have

$$D\left(\frac{\partial M}{\partial T}\right)_{H_0} = -\frac{dH_c}{dT} = \frac{S_p - S_a}{M_p - M_a}\,, \tag{26}$$

where in the last step we have used the modified Clausius-Clapeyron equation. We should remark that Eq. (26) and the continuity of the entropy on the boundary of the intermediate region are sufficient to obtain the entropy in the intermediate state. The relation $(\partial S/\partial H_0)_T = (\partial M/\partial T)_{H_0}$ can be integrated over H_0 when we realize that $(\partial M/\partial T)_{H_0}$ is independent of H_0 inside the intermediate state. Using the result that $S = S_a$ when $H_0 = H_c + DM_a$ we obtain Eq. (25).

By substituting Eq. (26) into Eq. (25) we may write the magnetization and entropy as

$$M = \alpha M_p + (1-\alpha)M_a\,, \tag{27}$$

$$S = \alpha S_p + (1-\alpha)S_a\,, \tag{28}$$

and interpret $\alpha = (M - M_a)/(M_p - M_a)$ as the fraction of the material in the paramagnetic state. If we consider the intermediate state to be made up of a large number of thin paramagnetic domains appearing when the applied field is large enough so that it is energetically favorable for a long needle to go into the paramagnetic state then Eqs. (27) and (28) are a natural starting point for the calculation.

We now calculate the heat capacity in the intermediate state and also the discontinuity in the heat capacity on going from the intermediate state to the PM or AF regions. Taking the temperature derivative of Eq. (28) at constant applied field and recalling that M_a, M_p, S_a, and S_p are functions of $H_c(T)$ and T, we obtain the heat capacity at constant applied field in the intermediate state,

$$C^I_{H_0} = C^a_{H_0} + DT\left[\left(\frac{\partial M}{\partial T}\right)_{H_0} - \left(\frac{\partial M_a}{\partial T}\right)_{H_0}\right]^2 \Big/ (1 - D\chi^a_T) + DT(M - M_a)\left(\frac{\partial^2 M}{\partial T^2}\right)_{H_0}\,, \tag{29}$$

where $C^a_{H_0}$ is the heat capacity in the AF state, and $\chi^a_T = (\partial M_a/\partial H_0)_T$ (see Appendix B for details). At the boundary of the intermediate state and the AF state the heat capacity is discontinuous. The discontinuity is given by

$$\Delta C_{H_0} = DT\left[\left(\frac{\partial M}{\partial T}\right)_{H_0} - \left(\frac{\partial M_a}{\partial T}\right)_{H_0}\right]^2 \Big/ (1 - D\chi^a_T)\,. \tag{30}$$

Equation (30) may be used to compare the discontinuity in heat capacity with the discontinuity in slope of magnetization as a function of temperature (see Figs. 11 and 4). We note that Eqs. (29) and (30) hold equally well for transitions into the second AF region or the PM region by replacing M_a, χ^a_T, and $C^a_{H_0}$ with M_p, χ^p_T, and $C^p_{H_0}$. The derivatives $(\partial M_a/\partial T)_{H_0}$ and χ^a_T in Eqs. (29) and (30) can be obtained from measurements on the sample with the same demagnetization factor.

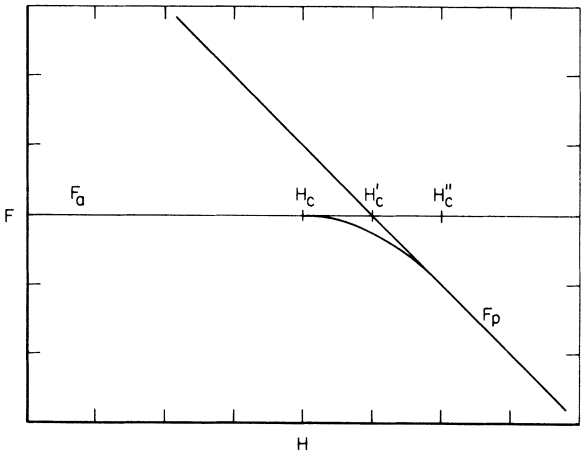

FIG. 10. Free energy at $T = 0$ of a sample having $DM_0/H_c(0) = \frac{1}{2}$. $H_c' = H_c + \frac{1}{2}DM_0$, $H_c'' = H_c + DM_0$. The minimum free energy between H_c and H_c'' is the intermediate state given by Eq. (22).

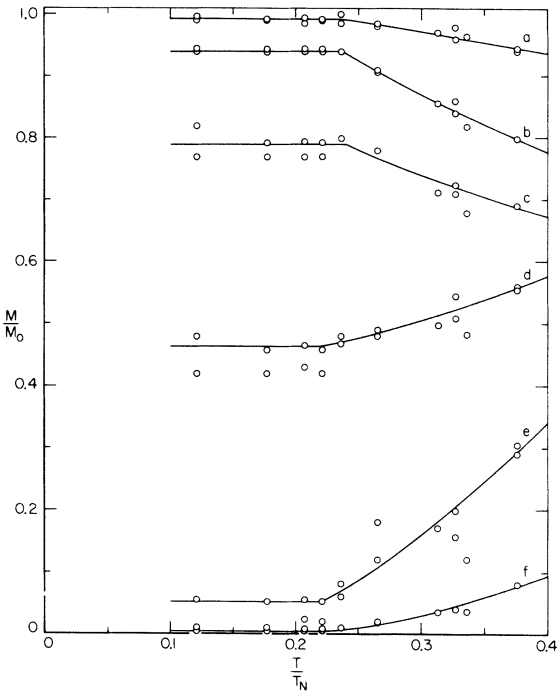

FIG. 11. Magnetization as a function of temperature for a $DyPO_4$ sample having $D \approx 1$, for different values of applied field H_0: *a*, 8 kG; *b*, 7 kG; *c*, 6.5 kG; *d*, 6 kG; *e*, 5.5 kG; *f*, 5.0 kG. The solid lines are fitted to the data shown.

In $DyPO_4$ the critical point occurs at a relatively low temperature and the critical field is approximately independent of temperature below the critical point. Using this approximation,

$$\frac{dH_c}{dT} = -D\left(\frac{\partial M}{\partial T}\right)_{H_0} \approx 0 ,$$

we have $C^I_{H_0} = C^a_{H_i} = C^p_{H_i}$, the heat capacity at constant internal field in the AF and PM regions, respectively, evaluated at $H_i = H_c$. While the approximation $dH_c/dT \to 0$ as $T \to 0$ must hold as required by the third law of thermodynamics and Eq. (26), a molecular-field model predicts a greater dependence of the critical field on temperature than is observed for $DyPO_4$. If we approximate $dH_c/dT \approx 0$, Eq. (29) becomes

$$C^I_{H_0} \approx C^a_{H_0} + DT\left[\left(\frac{\partial M_a}{\partial T}\right)_{H_0}\right]^2 \Big/ (1 - D\chi^a_T) , \qquad (31)$$

and Eq. (30) becomes

$$\Delta C_{H_0} \approx DT\left[\left(\frac{\partial M_a}{\partial T}\right)_{H_0}\right]^2 \Big/ (1 - D\chi^a_T) . \qquad (32)$$

Our measurements of the susceptibility for a long needle discussed in Sec. III indicated that the isothermal susceptibility approaches a sharp spike at low temperatures, but the measured susceptibility, while retaining the same general shape as the isothermal susceptibility, rapidly decreased in magnitude for $T \leq 1$ K and is zero within our accuracy of measurement for $T \leq 0.3$ K. This indicates that the adiabatic susceptibility χ_s is small at temperatures below 1 K and that our measured susceptibility was changing from the isothermal susceptibility to the adiabatic susceptibility in this temperature range. The molecular-field prediction in the PM region is that $\chi_s = 0$. If we make the further approximation $\chi_s \approx 0$, in addition to $dH_c/dT \approx 0$, we can further simplify Eqs. (31) and (32). Using the relation

$$C^a_{H_0}(\chi^a_T - \chi^a_s) = T\left[\left(\frac{\partial M_a}{\partial T}\right)_{H_0}\right]^2 , \qquad (33)$$

which also holds in the PM region with a replaced by p, Eq. (31) becomes

$$C^I_{H_0} \approx C^a_{H_0}\left(\frac{1 - D\chi^a_s}{1 - D\chi^a_T}\right) . \qquad (34)$$

Equation (32) is then

$$\Delta C_{H_0} \approx C^a_{H_0}\left(\frac{D(\chi^a_T - \chi^a_s)}{1 - D\chi^a_T}\right) = C^I_{H_0}\left(\frac{D(\chi^a_T - \chi^a_s)}{1 - D\chi^a_s}\right) , \qquad (35)$$

and with $\chi_s \approx 0$, we have

$$\Delta C_{H_0} \approx C^I_{H_0} D\chi^a_T . \qquad (36)$$

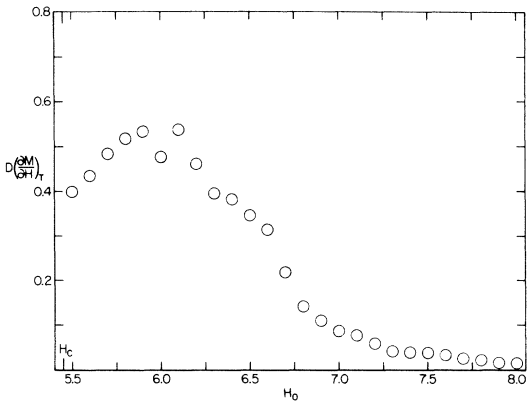

FIG. 12. $D(\partial M/\partial H_0)_T$ as a function of applied field (in kG) obtained from measurements of the magnetization as a function of applied field at $T = 0.80$ K.

All of the above equations hold equally well for transitions into the PM region if a is replaced by p. These equations may be used to relate experimentally determined quantities without using a model (such as a molecular-field approximation).

Experimentally, the boundary of the intermediate and paramagnetic states is independent of temperature within our accuracy in measuring the position of the heat-capacity maxima (see Fig. 4). This means that the application of Eq. (36) to the calculation of $\Delta C_{H_0}/C^I_{H_0}$ can be made by taking $(\partial M/dH_0)_T$ from one curve of $M(T)$ for the sample with $D = 1$ and T just higher than the intermediate to PM transition. We have used a measurement at $T = 0.8$ K to plot $D(\partial M/\partial H_0)_T$ in Fig. 12, and this behavior generally corresponds to the behavior of the heat capacity determined experimentally, although our samples were not ellipsoidal.

In the paramagnetic state there will be a maximum in the heat capacity arising from the alignment of an individual spin in the field of its neighbors plus the applied field. We shall refer to this maximum as the Schottky maximum. Through numerical calculation in the molecular-field approximation or the Bethe-Peierls approximation (the same as constant coupling for the Ising model), we see that in general in the paramagnetic region the position of this maximum increases in temperature as the applied field is increased. The peak also becomes broader as the field, and, hence, the temperature of the peak position, is increased.

In the molecular-field approximation, the heat capacity at constant applied field for a long needle in the paramagnetic state is given by

$$C^p_{H_0} = t\left(\frac{(1-\lambda)h - (1-2\lambda)m}{t}\right)^2 \left(\frac{(1-m^2)}{t + (1-2\lambda)(1-m^2)}\right) , \qquad (37)$$

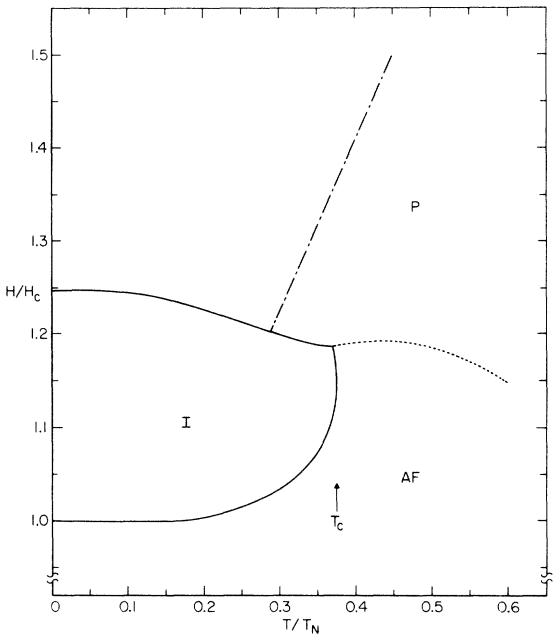

FIG. 13. Part of phase diagram of $DyPO_4$ in the molecular-field approximation for $D=1$ and $\lambda=0.34$. The solid line indicates the second-order transition dividing the intermediate region (I) from the paramagnetic region (P) and the antiferromagnetic region (AF). The dotted line is the second-order transition dividing the AF and PM states. The dot-dashed line is the locus of Schottky maxima in the heat capacity, not a true phase transition.

where $t=T/T_N$, $h=H_0/H_c$, and $m=M/M_0$. The temperature of the maximum in the heat capacity is given by

$$(1-\lambda)h=(1-2\lambda)m+\frac{t}{m}+\frac{(1-2\lambda)(1-m^2)}{2m}-\frac{(1-2\lambda)^2(1-m^2)^2}{2mt}\ . \quad (38)$$

For $DyPO_4$ ($\lambda=0.34$) with $D=0$, the curve of Schottky maxima in the applied field is nearly linear and intersects the first-order transition into the paramagnetic state at about $t=0.30$. The linear behavior arises primarily from the second term of Eq. (38) and $DyPO_4$ is fairly well approximated by the first two terms. Equation (38) still holds in the regions where the paramagnetic solution remains stable when the value of λ is reduced in accordance with Eqs. (9) and (8).

We shall therefore investigate the simplification in the theory when $dH_c/dT=0$. We have already seen that this implied $C^I_{H_c}=C^P_{H_c}$ which is given by Eq. (37) with $h=1$. Since we have seen that, within the molecular-field approximation, the heat capacity has a maximum intersecting the first-order-transition curve, we see that there is a Schottky maximum within the intermediate state and that this maximum occurs at the same temperature within the intermediate state independent of applied field. This maximum is not shown in Fig. 13 because dH_c/dT is not strictly zero within the molecular-field approximation and the Schottky maximum would have a temperature dependence within the intermediate state.

The expected behavior of the heat capacity at constant applied field is a broad Schottky maximum within the intermediate region followed by a discontinuity in the heat capacity given by Eq. (30) as the temperature is increased and the boundary of the intermediate region is crossed. Two maxima of this general description have been observed in dysprosium aluminum garnet by Keen, Landau, Schneider, and Wolf[15,22] for an applied field in the [111] direction. In the present experiment, however, only the positions of the maxima in heat capacity were measured, so that the nature of the anomaly could not be determined. It seems likely that the combination was taken as a single maximum in Fig. 3.

VI. DISCUSSION OF $D\approx 1$ RESULTS

A portion of the phase diagram for $DyPO_4$ calculated in the molecular-field approximation with $D=1$ is shown in Fig. 13, and a plot of the magnetization in the H-T plane is shown in Fig. 14. The values characterizing $DyPO_4$ are $\lambda=0.34$, $M_0=1.249$ kG.

The boundary of the intermediate state, labeled I in Fig. 13, is a line of second-order transitions into the PM and AF states. Associated with this transition we would expect a discontinuity in the derivative of the magnetization with respect to temperature at constant applied field and a discon-

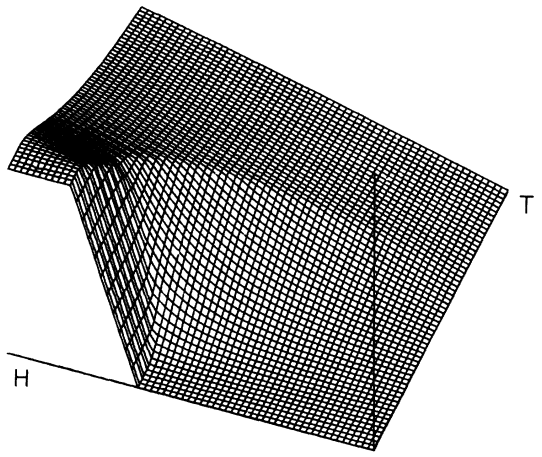

FIG. 14. Magnetization as a function of applied field and temperature in the molecular-field approximation for a $DyPO_4$ sample with $D=1$. We have taken $\lambda=0.34$. Maximum values shown are $H/H_c(0)=1.5$ and $T/T_N=1.5$. Viewing angles are $\theta=45°$ and $\varphi=200°$.

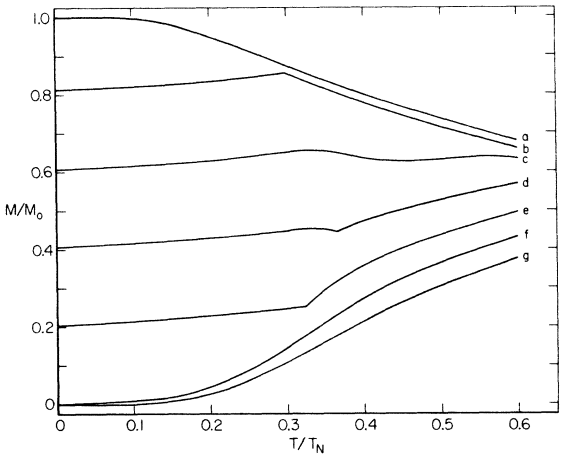

FIG. 15. Magnetization as a function of temperature in the molecular-field approximation with $D=1$, $\lambda=0.34$ for different values of applied field $H_0/H_c(0)$: *a*, 1.25; *b*, 1.20; *c*, 1.15; *d*, 1.10; *e*, 1.05; *f*, 1.00; *g*, 0.95.

tinuity in the heat capacity at constant applied field as given by Eq. (30). The dotted line gives the second-order phase transition between the AF and PM states, and the dot-dashed line gives the line of Schottky maxima in the heat capacity at constant applied field for $D=1$, and could be obtained from Eq. (32). These maxima do not represent a true phase transition and are analogous to the behavior of a ferromagnet in an applied field.

The experimentally determined magnetization as a function of temperature of a $DyPO_4$ sample with $D\approx 1$ is shown in Fig. 11 for fields ranging from 5.0 to 8.0 kG. We can see that there is a discontinuity in the derivative of the magnetization and that it occurs almost independently of applied field. Within the experimental accuracy, these discontinuities occur at the same temperature for a given applied field as do the heat-capacity peaks shown in Fig. 4. We also note that if the experimental values of $(\partial M/\partial T)_{H_0}$, $(\partial M_a/\partial T)_{H_0}$, and $(\partial M_a/\partial H_0)_T$ are used in Eq. (30) the magnitude of the discontinuity in the heat capacity decreases with increasing field for $H\gtrsim 1.15H_c(0)$ and this was observed in the measurements of heat-capacity maxima.

The molecular-field predictions for $DyPO_4$ with $D=1$ are shown in Fig. 15 for applied fields between $0.95H_c(0)$ and $1.25H_c(0)$. While we would not expect good quantitative agreement with Fig. 11, in this case the marked dissimilarity of the curves points up the unusual properties as measured experimentally. For example, while Figs. 4 and 11 agree quite well and indicate that the discontinuity in the derivative of the magnetization arises from a transition out of the intermediate state, the discontinuity in the derivative persists up to 8.0 kG which is greater than $H_c(0)+DM_0=6.70$ kG. In addition, the boundary of the intermediate region should be temperature dependent (see Figs. 13 and 10) for molecular-field prediction. The result that the discontinuity in the derivative of the magnetization persists to high fields may be stated another way: The magnetization does not saturate at $H=H_c(0)+DM_0$ even at very low temperatures, e.g., curve *b* of Fig. 11, while the magnetization curves for $D=0$ did saturate (Figs. 5 and 6). This means that if the experimental magnetization curves are plotted as a function of internal field we would not get one set of curves for all shapes. One explanation is that the samples used were not well approximated by ellipsoids.

The Schottky heat-capacity maxima in the H-T plane were obtained in the Bethe-Peierls approximation from a temperature derivative of Eq. (20) and the parameters appropriate for $DyPO_4$. A comparison of the positions of experimental and theoretical heat-capacity maxima in Fig. 16 indicates that the high-temperature heat-capacity maxima are indeed Schottky maxima. In addition, the calculated maxima become broader as the field is increased, as was observed experimentally.

VII. SUMMARY AND CONCLUSIONS

In summary, we have shown that the heat-capacity and magnetization results in applied fields for samples of $DyPO_4$ having demagnetizing factors $D\approx 1$ and $D\approx 0$ are qualitatively explained by the

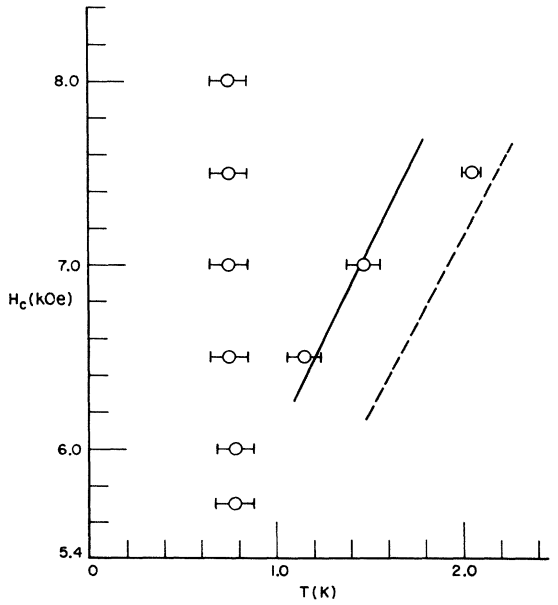

FIG. 16. Comparison of the Schottky maxima in the heat capacity predicted by the Bethe-Peierls approximation (solid lines) and molecular field (dashed line) using $J_a/k=1.25$ K, $M_0=1.249$ kG, and $D=1$ with experimental points for $DyPO_4$ with $D\approx 1$.

molecular-field and Bethe-Peierls approximations in which we have included dipolar interactions explicitly. It appears that the Bethe-Peierls approximation is somewhat better than the molecular-field approximation in representing the experimental results in the paramagnetic region.

Our measurements on samples with $D \approx 0$ indicate a first-order transition below a critical temperature T_c near 0.75 K. At higher temperatures the transition is of higher order. For temperatures less than T_c, the critical field is independent of temperature within our experimental accuracy. Our measurements on samples with $D \approx 1$ did not transform back into the results obtained on crystals with $D \approx 0$ when the appropriate transformations were made.[32,33] We believe that this is because of the nonellipsoidal shape of our samples.

We find that the molecular-field approximation, including dipolar interactions, gives the qualitative behavior of the heat-capacity peaks and for $D = 0$ predicts a first-order transition below a critical temperature as observed experimentally. Some details of the molecular-field predictions, such as a second-order transition for which the critical field increases with increasing temperature at low temperatures, have not been observed.

Our thermal and magnetization measurements on samples with $D \approx 1$ are consistent with each other, and from the magnetization results we have been able to calculate the observed heat-capacity maxima as a function of applied field and temperature. We conclude that for samples with $D = 1$ the lower-temperature branch of heat-capacity peaks in Fig. 4 arises from a transition from the intermediate state to the AF or PM state for a nonellipsoidal sample, and that the upper branch corresponds to the Schottky peaks of a paramagnet in a field. Measurements of the actual heat capacity in constant applied field for fields above $H_c(0)$ would be quite useful in checking these conclusions, as would measurements of magnetic properties or heat capacity on ellipsoidal samples. We have found it quite difficult, however, to obtain approximately ellipsoidal samples for large D because the crystals tend to cleave.

APPENDIX A

While the partial cancellation of the dipole sum on each sublattice with the sum of higher neighbor exchange interactions on the same sublattice shown in Table I is surprising, an even more surprising result is that the exchange interaction cancels a large part of the dipole interaction for the second through fifth neighbors individually as well.

The dipolar fields of the first ten neighbors are shown in Table I. The strongest dipolar interaction with a single spin which is not a nearest neighbor is with the fourth-nearest neighbors, the field arising from one of these neighbors being 817 G, while the field of a single second neighbor is 438 G. The lines observed spectroscopically in Ref. 3 were narrow enough, however, to have resolved any interaction from a single spin as large as 200 G.[35] The dipolar interaction with second and fourth neighbors must be largely canceled by exchange, therefore.

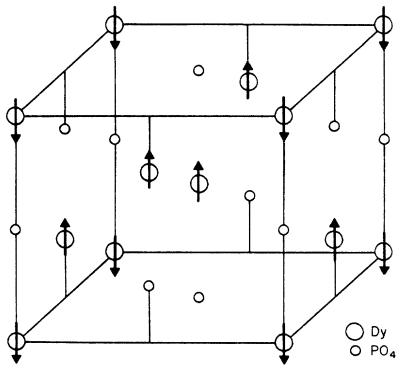

FIG. 17. A possible ferrimagnetic state of $DyPO_4$.

We also notice that the interactions with the third and fifth neighbors, which are both on the same sublattice as the central ion, are antiferromagnetic in sign. This suggests the possibility of ferrimagnetic states with saturation magnetization $M_s = \frac{1}{2} M_0$, consisting of planes of spins in the [001] (Fig. 17) or the [110] or [$1\bar{1}0$] directions (Fig. 18). Which of these states is stable near $H_c(0)$ will depend on the total interaction with third and fifth neighbors, the larger antiferromagnetic interaction leading to the stable state.

By combining these two states, that is, allowing spins to oppose the applied field only on every fourth [001] plane, and [or] on every fourth [110] plane it is possible to obtain ferrimagnetic states with $M_s = \frac{1}{4} M_0$ [$\frac{3}{4} M_0$]. For $DyPO_4$ at $T = 0$ and with dipolar interactions only, we would have

$$F(0) \leq -H_3 - H_5 \leq F(\tfrac{1}{4} M_0) \leq -H_5 \leq F(\tfrac{1}{2} M_0)$$
$$\leq +H_5 \leq F(\tfrac{3}{4} M_0) \leq H_3 + H_5$$
$$\leq F(M_0) ,$$

where the argument of the state F indicates the magnetization of the state, and for $DyPO_4$ $H_3 = 448$ G and $H_5 = 746$ G. The stable ferrimagnetic state with $M = \frac{1}{2} M_0$ is the one shown in Fig. 18.

While our magnetization measurements do give an indication of ferrimagnetic states near the critical field (see the bumps on the hysteresis curve Fig. 6), the extent in applied field of these states, if they do indeed exist, is less than 200 G, indicating that the third- and fifth-near-neighbor interac-

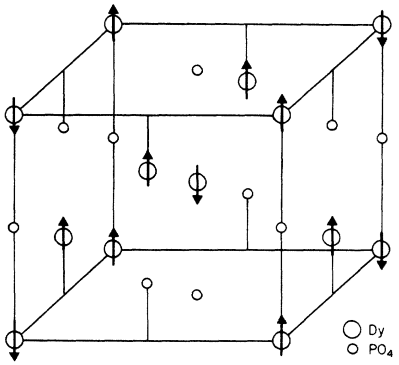

FIG. 18. A possible ferrimagnetic state of $DyPO_4$. Only $\frac{1}{4}$ of the new magnetic unit cell is shown.

tion is also largely canceled by exchange.

APPENDIX B

We shall derive Eq. (29) for the heat capacity at constant applied field in the intermediate state from the expression for the entropy in Eq. (25) or Eq. (28). Taking the derivative of Eq. (25) we obtain

$$C^I_{H_0}(H_0, T) = T\left(\frac{\partial S}{\partial T}\right)_{H_0}$$

$$= T\left(\frac{\partial S_a^*}{\partial T}\right)_{H_0} + TD\left(\frac{\partial M}{\partial T}\right)_{H_0}\left[\left(\frac{\partial M}{\partial T}\right)_{H_0} - \left(\frac{\partial M_a^*}{\partial T}\right)_{H_0}\right]$$

$$+ TD\left(\frac{\partial^2 M}{\partial T^2}\right)_{H_0}(M - M_a^*), \quad \text{(B1)}$$

where we have placed a star on S_a and M_a to emphasize that they are defined only on the boundary of the intermediate state, and the derivatives with respect to temperature must be expressed in terms of derivatives at constant internal field equal to the critical field $H_c(T)$. We have

$$\left(\frac{\partial S_a^*}{\partial T}\right)_{H_0} = \left(\frac{\partial S_a}{\partial H_i}\right)_T\left(\frac{\partial H_i^*}{\partial T}\right)_{H_0} + \left(\frac{\partial S_a}{\partial T}\right)_{H_i}, \quad \text{(B2)}$$

$$\left(\frac{\partial M_a^*}{\partial T}\right)_{H_0} = \left(\frac{\partial M_a}{\partial H_i}\right)_T\left(\frac{\partial H_i^*}{\partial T}\right)_{H_0} + \left(\frac{\partial M_a}{\partial T}\right)_{H_i}, \quad \text{(B3)}$$

where

$$\left(\frac{\partial H_i^*}{\partial T}\right)_{H_0} = \frac{dH_c}{dT} = -D\left(\frac{dM}{\partial T}\right)_{H_0}. \quad \text{(B4)}$$

Also,

$$\left(\frac{\partial S_a}{\partial T}\right)_{H_0} = \left(\frac{\partial S_a}{\partial H_i}\right)_T\left(\frac{\partial H_i}{\partial T}\right)_{H_0} + \left(\frac{\partial S_a}{\partial T}\right)_{H_i}, \quad \text{(B5)}$$

$$\left(\frac{\partial M_a}{\partial T}\right)_{H_0} = \left(\frac{\partial M_a}{\partial H_i}\right)_T\left(\frac{\partial H_i}{\partial T}\right)_{H_0} + \left(\frac{\partial M_a}{\partial T}\right)_{H_i}, \quad \text{(B6)}$$

and

$$\left(\frac{\partial H_i}{\partial T}\right)_{H_0} = -D\left(\frac{\partial M_a}{\partial T}\right)_{H_0}. \quad \text{(B7)}$$

Combining Eqs. (B2)–(B7) we have

$$\left(\frac{\partial S_a^*}{\partial T}\right)_{H_0} = \left(\frac{\partial S_a}{\partial T}\right)_{H_0} + D\left(\frac{\partial S_a}{\partial H_i}\right)_T\left[\left(\frac{\partial M_a}{\partial T}\right)_{H_0} - \left(\frac{\partial M}{\partial T}\right)_{H_0}\right], \quad \text{(B8)}$$

$$\left(\frac{\partial M_a^*}{\partial T}\right)_{H_0} = \left(\frac{\partial M_a}{\partial T}\right)_{H_0} + D\left(\frac{\partial M_a}{\partial H_i}\right)_T\left[\left(\frac{\partial M_a}{\partial T}\right)_{H_0} - \left(\frac{\partial M}{\partial T}\right)_{H_0}\right]. \quad \text{(B9)}$$

Using the Maxwell relation $(\partial S_a/\partial H_0)_T = (\partial M_a/\partial T)_{H_0}$, we obtain

$$\left(\frac{\partial S_a}{\partial H_i}\right)_T = \left(\frac{\partial M_a}{\partial T}\right)_{H_0}\Big/\left(\frac{\partial H_i}{\partial H_0}\right)_T, \quad \text{(B10)}$$

$$\left(\frac{\partial M_a}{\partial H_i}\right)_T = \left(\frac{\partial M_a}{\partial H_0}\right)_T\Big/\left(\frac{\partial H_i}{\partial H_0}\right)_T, \quad \text{(B11)}$$

and with $(\partial H_i/\partial H_0)_T = 1 - D(\partial M_a/\partial H_0)_T$ we obtain

$$\left(\frac{\partial S_a^*}{\partial T}\right)_{H_0} = \left(\frac{\partial S_a}{\partial T}\right)_{H_0} + D\left(\frac{\partial M_a}{\partial T}\right)_{H_0}\left[\left(\frac{\partial M_a}{\partial T}\right)_{H_0} - \left(\frac{\partial M}{\partial T}\right)_{H_0}\right]\Big/\left[1 - D\left(\frac{\partial M_a}{\partial H_0}\right)_T\right], \quad \text{(B12)}$$

$$\left(\frac{\partial M_a^*}{\partial T}\right)_{H_0} = \left(\frac{\partial M_a}{\partial T}\right)_{H_0} + D\left(\frac{\partial M_a}{\partial H_0}\right)_T\left[\left(\frac{\partial M_a}{\partial T}\right)_{H_0} - \left(\frac{\partial M}{\partial T}\right)_{H_0}\right]\Big/\left[1 - D\left(\frac{\partial M_a}{\partial H_0}\right)_T\right]. \quad \text{(B13)}$$

Substituting Eqs. (B12) and (B13) into Eq. (B1) and collecting terms we obtain Eq. (29).

[1]G. A. Prinz (private communication).
[2]J. H. Colwell, B. W. Mangum, D. D. Thornton, J. C. Wright, and H. W. Moos, Phys. Rev. Letters 23, 1245 (1969).
[3]J. C. Wright, H. W. Moos, J. H. Colwell, B. W. Mangum, and D. D. Thornton, Phys. Rev. B 3, 843 (1971).
[4]G. T. Rado, Solid State Commun. 8, 1349 (1970).
[5]J. W. Essam and M. F. Sykes, Physica 29, 378 (1963).
[6]M. F. Sykes, J. W. Essam, and D. S. Gaunt, J. Math. Phys. 6, 283 (1965).

[7]D. S. Gaunt and C. Domb, J. Phys. C 1, 1038 (1968).
[8]C. S. Koonce, B. W. Mangum, and D. D. Thornton, in *Proceedings of the Twelfth International Conference on Low Temperature Physics*, edited by E. Kanda (Keigaku, Tokyo, 1971).
[9]R. W. G. Wycoff, *Crystal Structures*, 2nd ed. (Interscience, New York, 1965), Chap. VIII.
[10]K. Motizuki, J. Phys. Soc. Japan 14, 759 (1959).
[11]J. Kanamori, Progr. Theoret. Phys. (Kyoto) 20, 890 (1958).
[12]C. J. Gorter and T. Van Peski-Tinbergen, Physica 22, 273 (1956).
[13]M. Ball, W. P. Wolf, and A. F. G. Wyatt, Phys. Letters 10, 7 (1964).
[14]H. W. Capel, Physica 31, 1152 (1965).
[15]B. E. Keen, D. P. Landau, B. Schneider, and W. P. Wolf, J. Appl. Phys. 37, 1120 (1966).
[16]B. E. Keen, D. P. Landau, and W. P. Wolf, Phys. Letters 23, 202 (1966).
[17]W. P. Wolf, in *Critical Phenomena*, edited by M. S. Green and J. V. Sengers, Natl. Bur. Std. (U.S.) Misc. Publ. 273 (U.S. GPO, Washington, D. C., 1965), p. 49.
[18]R. Bidaux and B. Vivet, J. Phys. 29, 57 (1968).
[19]R. Bidaux, P. Carrara, and B. Vivet, J. Phys. 29, 357 (1968).
[20]I. S. Jacobs and P. E. Lawrence, Phys. Rev. 164, 866 (1967).
[21]V. A. Schmidt and S. A. Friedberg, Phys. Rev. B 1, 2250 (1970).
[22]D. P. Landau, B. E. Keen, B. Schneider, and W. P. Wolf, Phys. Rev. B 3, 2310 (1971).
[23]M. E Fisher, Proc. Roy. Soc. (London) A254, 66 (1960).
[24]P. W. Kasteleijn, Physica 22, 387 (1956).
[25]B. R. Heap, Proc. Phys. Soc. (London) 80, 248 (1962).
[26]S. Yomosa, J. Phys. Soc. Japan 15, 1068 (1960).
[27]R. S. Feigelson, J. Am. Ceram. Soc. 47, 257 (1964).
[28]B. W. Mangum and D. D. Thornton, Rev. Sci. Instr. 41, 1764 (1970).
[29]F. G. Brickwedde, H. Van Dijk, M. Durieux, J. R. Clement, and J. K. Logan, Natl. Bur. Std. (U.S.) Monograph No. 10 (U.S. GPO, Washington, D. C., 1960).
[30]Certain commercial equipment, instruments, or materials are identified in this paper in order to adequately specify the experimental procedure. In no case does such identification imply recommendation or endorsement by the National Bureau of Standards, nor does it imply that the material or equipment is necessarily the best available for the purpose.
[31]L. Holmes, R. Sherwood, and L. G. Van Uitert, J. Appl. Phys. 39, 1373 (1968).
[32]P. M. Levy and D. P. Landau, J. Appl. Phys. 39, 1128 (1968).
[33]P. M. Levy, Phys. Rev. 170, 595 (1968).
[34]A. F. G. Wyatt, J. Phys. C 1, 684 (1968).
[35]J. C. Wright (private communication).

PHYSICAL REVIEW B VOLUME 4, NUMBER 11 1 DECEMBER 1971

Measurement of Conduction-Electron Spin-Density Oscillations in Ordered *Fe*Si Alloys

Mary Beth Stearns
Scientific Research Staff, Ford Motor Company, Dearborn, Michigan 48121
(Received 1 February 1971; revised manuscript received 13 May 1971)

Pulsed NMR hyperfine field measurements have been made on ordered $Fe_{1-x}Si_x$ alloys for $0.181 \leq x \leq 0.249$. Using ordered compounds greatly improves the accuracy with which internal-field shifts due to the first nine neighbor shells can be measured. A number of effects which were difficult to observe in dilute alloys are easily measurable. Dipolar structure and saturation or shielding effects are seen for various neighbor shells. We see no damping of the spin density oscillations with alloying. This allows the determination of a lower limit for the mean free path of the conduction electrons in the alloys. The third-, fourth-, and sixth-nearest-neighbor Fe atoms give positive polarizations. The measured hyperfine field shifts are extrapolated and combined with dilute alloy data to obtain the spin-density oscillations surrounding an Fe atom in pure Fe.

I. INTRODUCTION

In metals ferromagnetism is believed to be achieved by the "local" atomic moments being aligned through the intermediary of the polarized "itinerant" electrons.[1] Many experiments and calculations have been carried out in recent years to investigate this interaction. For a discussion of these see the Introduction in the following paper, hereafter referred to as Paper II. The experiments which yield by far the most direct information about the spin density of the itinerant s-like conduction electrons are Mössbauer[2,3] and NMR[4-6] experiments.

A properly chosen system (namely, an alloy system where the solute atom has *no* moment and the form factor of the Fe atoms does not change upon alloying) can give detailed information about the variation of the s-like conduction-electron polarization (CEP) with distance around an Fe atom.

We report on accurate measurements of the hyper-